ACS central science

Research Article

http://pubs.acs.org/journal/acscii

A Nano-In-Micro System for Enhanced Stem Cell Therapy of Ischemic Diseases

Hai Wang,[†,‡,§,◆] Pranay Agarwal,[†,§,◆] Yichao Xiao,[§,∥,#,◆] Hao Peng,[†,⊥] Shuting Zhao,[†,§] Xuanyou Liu,[§,∥] Shenghua Zhou,[#] Jianrong Li,[▽] Zhenguo Liu,[*,§,∥] and Xiaoming He[*,†,‡,§]

[†]Department of Biomedical Engineering, [‡]Comprehensive Cancer Center, [§]Davis Heart and Lung Research Institute, and [∥]Division of Cardiovascular Medicine, and [▽]Department of Veterinary Biosciences, The Ohio State University, Columbus, Ohio 43210, United States

[⊥]Department of Burns and Plastic Surgery, The Third Xiangya Hospital and [#]Department of Cardiology, The Second Xiangya Hospital, Central South University, Changsha, Hunan 410013, P.R. China

S *Supporting Information*

ABSTRACT: Stem cell therapy holds great potential for treating ischemic diseases. However, contemporary methods for local stem cell delivery suffer from poor cell survival/retention after injection. We developed a unique multiscale delivery system by encapsulating therapeutic agent-laden nanoparticles in alginate hydrogel microcapsules and further coentrapping the nano-in-micro capsules with stem cells in collagen hydrogel. The multiscale system exhibits significantly higher mechanical strength and stability than pure collagen hydrogel. Moreover, unlike nanoparticles, the nano-in-micro capsules do not move with surrounding body fluid and are not taken up by the cells. This allows a sustained and localized release of extracellular epidermal growth factor (EGF), a substance that could significantly enhance the proliferation of mesenchymal stem cells while maintaining their multilineage differentiation potential via binding with its receptors on the stem cell surface. As a result, the multiscale system significantly improves the stem cell survival at 8 days after implantation to ∼70% from ∼4−7% for the conventional system with nanoparticle-encapsulated EGF or free EGF in collagen hydrogel. After injecting into the ischemic limbs of mice, stem cells in the multiscale system facilitate tissue regeneration to effectively restore ∼100% blood perfusion in 4 weeks without evident side effects.

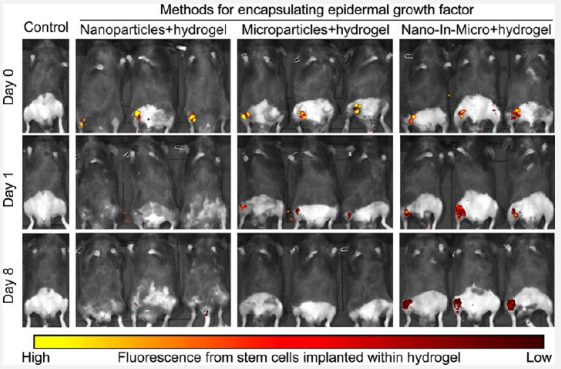

INTRODUCTION

Ischemic tissue diseases are a major cause of morbidity and mortality worldwide.[1−3] For therapy of the tissue ischemia, efficient restoration of blood perfusion is crucial to prevent tissue necrosis.[4,5] Unfortunately, due to the limitations of contemporary therapeutic approaches, there is an urgent need for effective and safe therapies to regenerate or repair ischemic tissue quickly.[6] One of the most promising approaches is stem cell-based therapy.[7−9] Stem cells can be used to restore tissue/organ function via either direct differentiation or production of various bioactive substances (e.g., cytokines and growth factors) in the damaged tissue/organ.[10,11] However, stem cell therapy remains elusive due to the poor *in vivo* survival of the cells after implantation.[12−16] Less than ∼10% of implanted cells could remain in the initial target tissue including ischemic limb after approximately 1−7 days.[17−22]

To improve the cell retention and survival at the injection site, stem cells may be delivered within a fluid material (e.g., collagen solution, a major protein in the extracellular matrix of mammalian tissues) that can form a hydrogel after injection (Figure S1a). Moreover, maintaining an appropriate level of growth factors in the microenvironment is necessary to promote the cell retention/survival/proliferation.[23] However, growth factors (e.g., epidermal growth factor or EGF) are not stable and can be degraded within a few hours when they are exposed to body fluid *in vivo*.[24] Nanoparticles have been used as the carrier to protect and deliver macromolecules including proteins *in vivo*.[25,26] Unfortunately, nanoparticles are most suitable for intracellular delivery because cells can readily take up nanoparticles. This can certainly compromise the actions of growth factors (e.g., EGF) that function by interacting with their target molecules (e.g., receptors) on the outer surface of stem cells (Figure S1b). To address this challenge, a nano-in-micro capsule is developed in this study for encapsulating EGF to achieve a sustained and localized release of the growth factor inside collagen hydrogel (Figure S1c). EGF was chosen in the present study because, unlike many other growth factors such as vascular endothelial growth factor (VEGF) and transforming growth factor-beta (TGF-β), EGF could significantly enhance the proliferation of mesenchymal stem cells while maintaining their multilineage differentiation potential.[27,28] EGF was

Received: May 18, 2017
Published: July 19, 2017

DOI: 10.1021/acscentsci.7b00213
ACS Cent. Sci. 2017, 3, 875−885

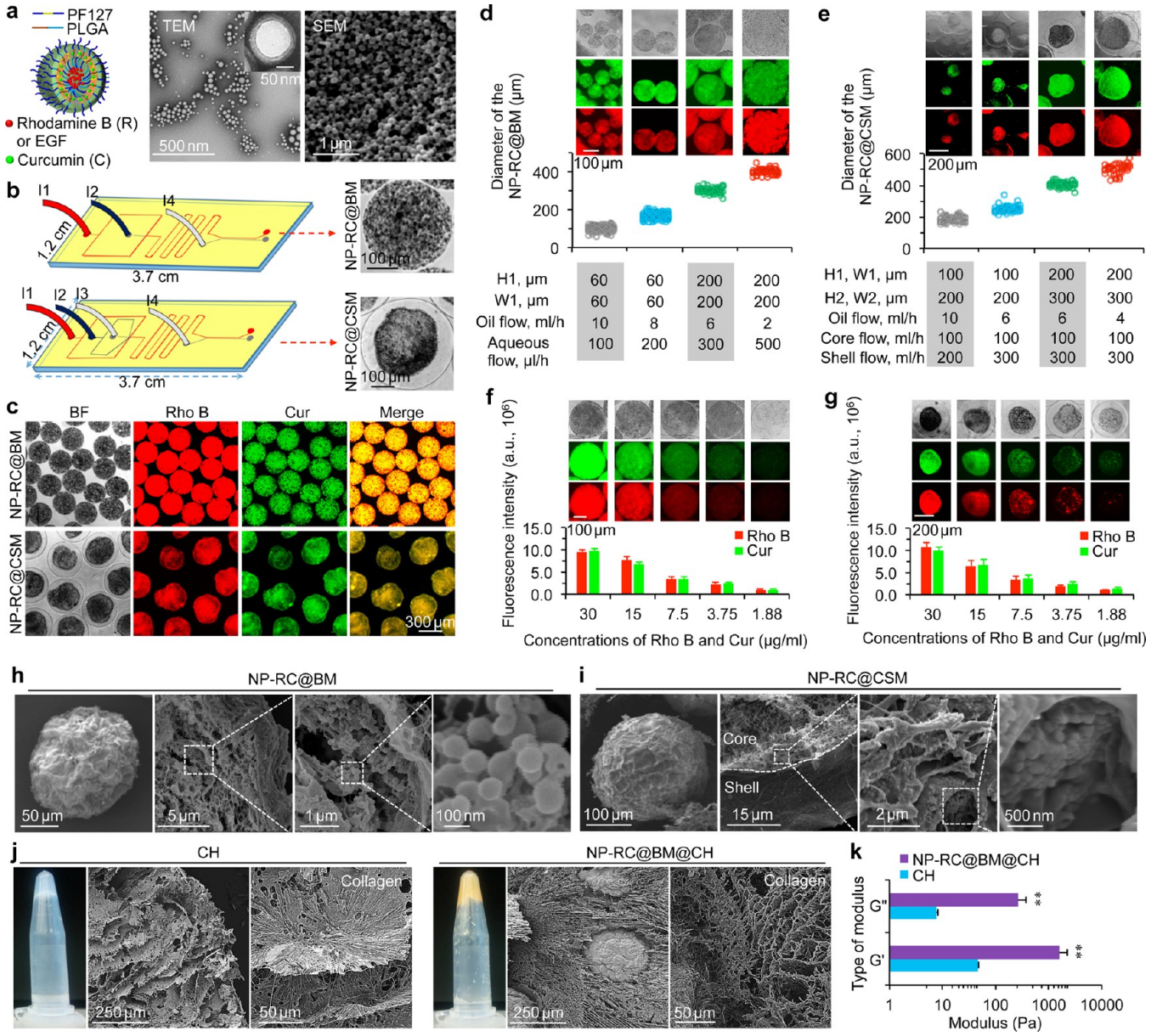

Figure 1. Fabrication and characterization of the multiscale composite system. (a) A schematic illustration of the nanoparticle (NP) encapsulated with both hydrophilic rhodamine B (Rho B or R) and hydrophobic curcumin (Cur or C). The nanoparticles were therefore called NP-RC. Also shown are typical transmission and scanning electron microscopy (TEM and SEM) images of the nanoparticles. The inset shows the core−shell structure of the nanoparticles. (b) Schematics of the microfluidic systems used for producing NP-RC encapsulated bead microcapsules (NP-RC@BM, top) and core−shell microcapsules (NP-RC@CSM, bottom). (c) Bright field (BF) and fluorescence images of NP-RC@BM and NP-RC@CSM showing successful encapsulation of Rho B (red) and Cur (green) in the nano-in-micro capsules. NP-RC distributed throughout the BM, but in only the core of the CSM. (d−e) Controlled fabrication of the nano-in-micro capsules: The diameter of the NP-RC@BM (d) and NP-RC@CSM (e) could be precisely controlled. H: height and W: width (see Figure S3 for the detailed information on the height and width of the devices). (f−g) The concentration of Rho B and Cur in NP-RC@BM (f) and NP-RC@CSM (g) could be precisely controlled. (h) SEM images of dried NP-RC@BM showing NP-RC inside the capsules. (i) SEM images of dried NP-RC@CSM showing the core−shell structure, as well as NP-RC in the core of the capsules. (j) Macroscopic (in centrifuge tube) and microscopic SEM images of the collagen hydrogel (CH) and NP-RC@BM in CH (NP-RC@BM@CH) showing the NP-RC@BM@CH has more homogeneous microstructure than CH. (k) Data of storage (G') and loss (G'') moduli showing the NP-RC@BM@CH has stronger and more stable structure than CH. Error bars represent ± standard deviation (s.d., $n = 3$). $^{**}p < 0.01$ (Mann−Whitney U-test).

encapsulated inside the nanoparticles first, and the resultant EGF-laden nanoparticles were further encapsulated within alginate hydrogel microcapsules. Because of their large size (~300 μm), cells could not uptake the nano-in-micro capsules, while the nanoparticles inside the capsules provided long-term protection to the encapsulated EGF. Finally, we integrated the EGF-laden nano-in-micro capsules and human adipose-derived stem cells (ADSCs, stromal cells from adipose tissues with great potential for clinical applications) into collagen hydrogel to form a multiscale composite system for implantation by local injection to treat ischemic injury in the limb.

RESULTS AND DISCUSSION

Fabrication and Characterization of the Multiscale System. To generate the multiscale system, we prepared nanoparticles of Pluronic F127 (PF127) and poly(lactic-*co*-

DOI: 10.1021/acscentsci.7b00213
ACS Cent. Sci. 2017, 3, 875−885

glycolic acid) (PLGA) first, using an improved double emulsion method.[29−31] For visualization and characterization of the nanoparticles, we encapsulated two fluorescent dyes, rhodamine B (R, hydrophilic) and curcumin (C, hydrophobic) in the nanoparticles. By adjusting the feeding ratio of rhodamine B to curcumin based on their encapsulation efficiency (EE, Figure S2), their amount in the nanoparticles was controlled to be the same for the characterization studies. As illustrated schematically in Figure 1a, rhodamine B and curcumin were encapsulated in the hydrophilic core and hydrophobic shell of the nanoparticles (NP-RC), respectively. Typical transmission and scanning electron microscopy (TEM and SEM) images showing a core−shell structure, uniform size, and spherical morphology of the NP-RC are given in Figure 1a. The nano-in-micro capsules were prepared by using microfluidic flow-focusing devices (Figure 1b), similarly to what we did before (albeit no nanoparticles).[32] The NP-RC can be distributed throughout the bead microcapsule (NP-RC@BM) or only in the core of core−shell microcapsules (NP-RC@CSM) by using microfluidic devices of different designs (Figures 1b and S3). For the microfluidic devices, I1 is the inlet of the oil phase. Alginate from the I2 inlet was used to fabricate the bead microcapsules (BMs) or the shell of the core−shell microcapsules (CSMs) because of its biocompatibility and reversible gelation with divalent cations such as Ca^{2+} under mild conditions that are not harmful to living cells.[33−37] Another biocompatible polymer (carboxymethyl cellulose) was added in the core fluid (from the I3 inlet) to increase its viscosity, which is necessary for fabricating the NP-RC@CSM.[32,38] The aqueous extraction fluid (which is the same as the core fluid in terms of composition) was introduced into the microfluidic devices from I4 to efficiently extract microcapsules from the oil phase into isotonic aqueous solution. As shown in Figure 1c, the red fluorescence of rhodamine B and green fluorescence of curcumin colocalized and distributed homogeneously in the BMs or the core of CSMs. However, when we used microcapsules to encapsulate free (i.e., without nanoparticle encapsulation) rhodamine B directly (note: curcumin is a hydrophobic agent that cannot be encapsulated directly in the alginate hydrogel microcapsules), nearly all the rhodamine B was released into mannitol solution outside the microcapsules as soon as we collected microcapsules (Figure S4). This is not surprising as the pore size of the alginate bead microcapsules are much bigger than the size of rhodamine B.[39,40]

Furthermore, we generated nano-in-micro capsules of various sizes (100−500 μm in diameter) with low polydispersity (Figure 1d−e). This was achieved by tuning the flow rates of oil and aqueous core and/or shell flows, and the dimensions of the microfluidic channel (Figure S3). Overall, the size of the nano-in-micro capsules increases with the decrease of the oil flow rate and the increase of aqueous core and shell flow rates. However, the maximum size of the nano-in-micro capsules is determined by the dimensions of the microfluidic channel. We were also able to accurately control the drug concentration in the nano-in-micro capsules (Figure 1f−g). During the formation of nano-in-micro capsules, isotonic mannitol solution was used for collection and purification of the capsules. We found that the amount of rhodamine B or curcumin in the mannitol solution for collecting the nano-in-micro capsules was negligible (Figure S5). Therefore, independent of the concentration of agents in the capsules, the encapsulation efficiency (EE) of the nanoparticles in the microcapsules was 100% (Figure S5). This is in stark contrast to the nearly zero EE shown in Figure S4 for encapsulating free rhodamine B in the alginate hydrogel microcapsules. This also allows precise control of the amount of rhodamine B and curcumin in the nano-in-micro capsules by using different amounts of the agents-laden nanoparticles for producing the capsules. The amount of rhodamine B and curcumin in the nanoparticles could be accurately calculated using the encapsulation efficiency data shown in Figure S2. The morphology of the nano-in-micro capsules was determined by using SEM. For NP-RC@BM, the size was ∼150 μm after drying (Figure 1h). Inside the capsules, the alginate matrix is visible, as well as the nanoparticles. The core−shell structure of NP-RC@CSM could be readily identified in the SEM image, and nanoparticles could be seen inside the core of the capsules (Figure 1i).

We next investigated the stability and drug release behavior of the nano-in-micro capsules in cell culture medium. As shown in Figures S6 and S7, both NP-RC@BM and NP-RC@CSM are stable in medium. The fluorescence intensity of rhodamine B and curcumin gradually increases in the surrounding medium with time, indicating gradual release of the two agents from the nano-in-micro capsules into medium. It is worth noting that the nano-in-micro capsules could be freeze-dried for long-term storage without altering its morphology and property after rehydration (Figure S8). Since more nanoparticles could be encapsulated in the BM than CSM given the same size, the BM-based nano-in-micro capsules were utilized for further characterization and therapy studies.

Next, we integrated the BM-based nano-in-micro capsules and stem cells into collagen hydrogel (CH) to form a multiscale composite system. The structures of both the pure CH and NP-RC@BM assembled in CH (NP-RC@BM@CH) are shown in Figure 1j. Interestingly, the collagen matrix in the NP-RC@BM@CH exhibited a more homogeneous microstructure than that in pure CH, indicating the microcapsules could alter the distribution and orientation of the collagen fibers during the gelling process. This homogeneous structure with fine voids could make the RC@BM@CH stronger and more stable than pure CH that is heterogeneous with both fine and large voids. In addition, the capsules can work as the skeleton to support and strengthen the structure of the collagen hydrogel, because the alginate hydrogel in the microcapsules are much stronger than the collagen hydrogel (Figures 1k and S9). Indeed, both the storage (G') and loss (G'') moduli of NP-RC@BM@CH were much higher than that of CH (Figure 1k). However, the nanoparticles (NP-RC) showed no significant impact on the mechanical properties of alginate hydrogel or carboxymethyl cellulose solution in the nano-in-micro capsules (Figure S9).

Sustained Release of EGF and High Cell Survival in the Multiscale System. To assess the capability of the multiscale system in promoting cell survival and proliferation *in vitro*, EGF was encapsulated (similarly to rhodamine B) in the nano-in-micro capsules with an EE of ∼74% (Figure S2). It is worth noting that EGF was dissolved in deionized water rather than organic solvent (dichloromethane) during its encapsulation in nanoparticles using the aforementioned double emulsion method. The resultant nanoparticles had an aqueous core containing EGF and a polymer shell (Figure 1a). The organic solvent for dissolving the polymer was removed from the polymer shell immediately after the double-emulsion process by rotary evaporation. Others have also used this method for protein encapsulation.[41−43] The EGF-laden nanoparticles were dispersed in aqueous solution during microfluidic production of the nano-in-micro capsules, as well. Therefore, contact between EGF and organic solvent was negligible during the entire procedure of

DOI: 10.1021/acscentsci.7b00213
ACS Cent. Sci. 2017, 3, 875−885

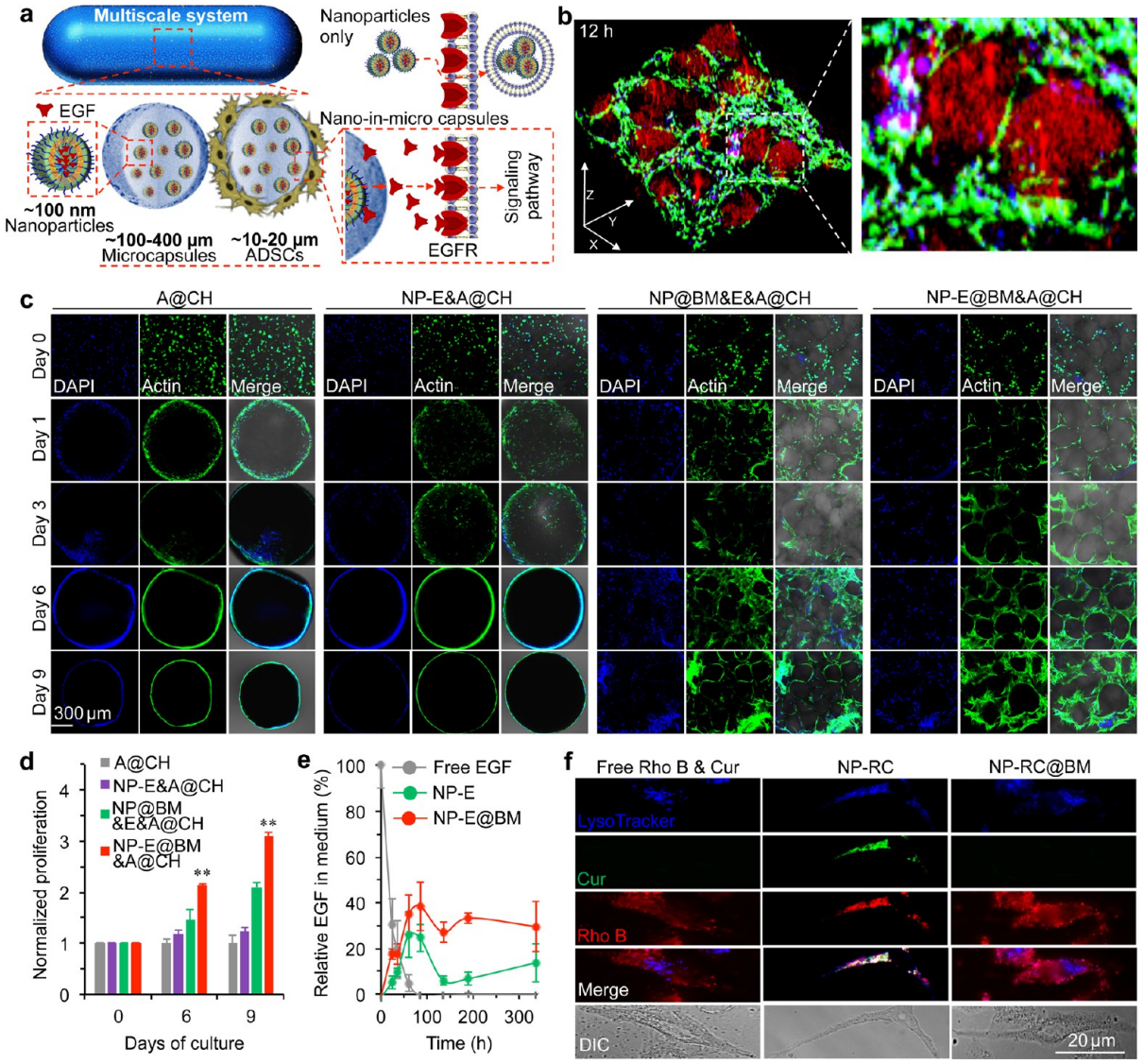

Figure 2. Significantly enhanced survival and proliferation of ADSCs in the multiscale composite system. (a) A schematic illustration of the multiscale system showing controlled release of extracellular epidermal growth factor (EGF) to interact with the EGF receptors (EGFRs) on the cell plasma membrane. (b) 3D confocal images of the multiscale system after 12 h of culture showing that ADSCs grow homogeneously in the space between the nano-in-micro capsules. Most rhodamine B (Rho B) stayed in the nanoparticles inside the capsules, while some was released and entered the cells. (c) Confocal images of ADSCs (A) in collagen hydrogel (CH) (A@CH), EGF (E) encapsulated nanoparticles (NP-E) and ADSCs in CH (NP-E&A@CH), empty nano-in-micro capsules mixed with free EGF and ADSCs in CH (NP@BM&E&A@CH), and EGF encapsulated nano-in-micro capsules and ADSCs in CH (NP-E@BM&A@CH). The data show that both A@CH and NP-E&A@CH shrink greatly and cells migrate out of both systems. The cells distributed homogeneously only in the NP-E@BM&A@CH. (d) Proliferation of ADSCs in A@CH, NP-E&A@CH, NP@BM&E&A@CH, and NP-E@BM&A@CH on days 0, 6, and 9. Error bars represent s.d. ($n = 3$). $^{**}p < 0.01$ (Kruskal–Wallis H-test). (e) Sustained release of EGF from NP-E and NP-E@BM into medium together with the stability of free EGF in medium at 37 °C. (f) Cellular uptake of free rhodamine B and curcumin (Rho B & Cur), rhodamine B and curcumin encapsulated in nanoparticles (NP-RC), and rhodamine B and curcumin encapsulated in nano-in-micro capsules (NP-RC@BM), showing the distribution of the two agents in cells incubated with NP-RC@BM is similar to that in cells incubated with free Rho B & Cur. In contrast, their distribution in NP-RC treated cells is colocalized with lysoTracker, indicating the cells could take up NP-RC via endocytosis, but not NP-RC@BM. The agents are released from NP-RC@BM before entering the cells.

its encapsulation and release. This ensured the EGF to retain its intact structure after releasing from the nano-in-micro capsules, which was confirmed by UV–Vis and circular dichroism (CD) spectroscopy studies. As shown in Figure S10, the free EGF and EGF released from nano-in-micro capsules have similar spectra of UV–Vis (with an absorbance peak at 280 nm, Figure S10a) and CD (with a negative band at ~202 nm and a positive one at ~230 nm similar to that published in the literature,[44,45] Figure S10b). The intact function of the EGF released from nano-in-micro capsules was further confirmed by its capability of enhancing cell survival and proliferation, as detailed below.

The EGF-laden nano-in-micro capsules and ADSCs were then assembled together in CH by mixing them in collagen solution for gelling at 37 °C. We hypothesized that the EGF could be released slowly from the nano-in-micro capsules and bind to the EGF receptor (EGFR) on the outer plasma membrane of ADSCs (Figure 2a). Moreover, the CH reinforced by the nano-in-micro capsules could provide a three-dimensional (3D) scaffold for cell adhesion and proliferation (Figure 2a). To test the hypothesis,

DOI: 10.1021/acscentsci.7b00213
ACS Cent. Sci. 2017, 3, 875–885

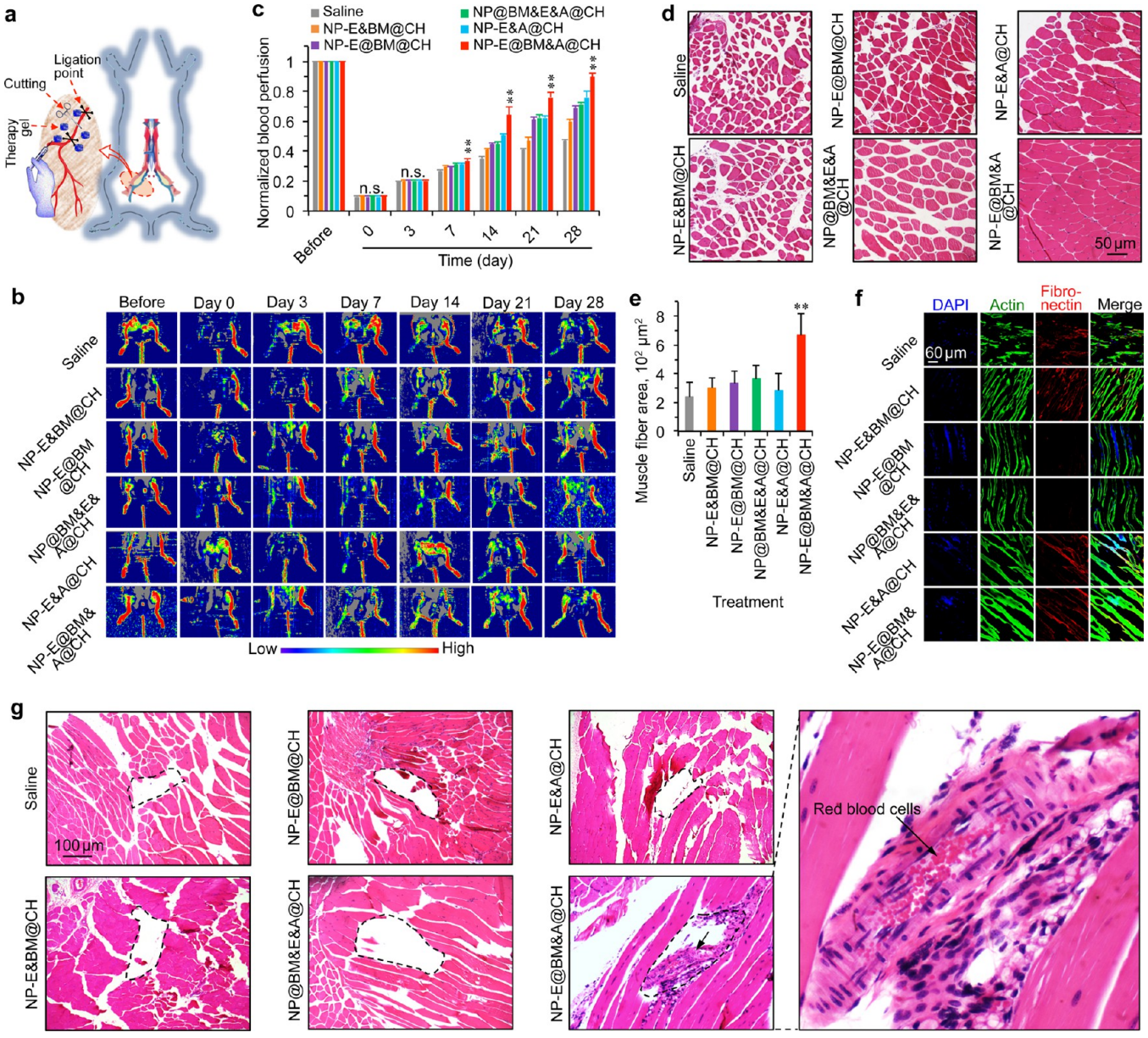

Figure 3. Significantly enhanced regeneration of ischemic limb with the multiscale composite system. (a) A schematic illustration of the hind limb ischemia model created by unilateral femoral artery ligation together with the injection sites (blue dots). (b) Laser Doppler perfusion imaging (LDPI) images of the regional blood flow in both limbs of the mice. The blood perfusion in right limb reduced dramatically after induction of ischemia, indicating successful surgery. After treatment with saline, NP-E and microcapsules in CH (NP-E&BM@CH), NP-E@BM in CH (NP-E@BM@CH), NP@BM with free EGF and ADSCs in CH (NP@BM&E&A@CH), NP-E with ADSCs in CH (NP-E&A@CH), and NP-E@BM with ADSCs in CH (NP-E@BM&A@CH), recovery of blood perfusion was better for the mice treated with NP-E@BM&A@CH than all the other control formulations. (c) Quantitative data from the LDPI images showing the blood perfusion in the right hind limb of NP-E@BM&A@CH treated mice were significantly higher than that of mice from all the other groups after day 7. Error bars represent s.d. ($n = 5$). $^{**}p < 0.01$ (one-way ANOVA followed by post hoc conservative Tukey's test). (d–e) Hematoxylin and eosin (H&E) staining (d) and average muscle fiber area (e) of the mice with different treatments showing ~100% restoration of blood perfusion after 4 weeks without compromising the host muscle fibers by the NP-E@BM&A@CH treatment. Error bars represent s.d. ($n = 50$). $^{**}p < 0.01$ (Kruskal–Wallis H-test). (f) Confocal images of actin and fibronectin of mice with different treatments showing the NP-E@BM&A@CH treated mice have longer and larger muscle fiber. (g) H&E staining of tissue from the injection area in mice with different treatments showing newly formed blood vessels could only be observed for the NP-E@BM&A@CH treated mice. The areas enclosed in the dashed lines are injection sites for the different treatments.

we first encapsulated both rhodamine B and EGF in the nano-in-micro capsules for visualization. After 12 h of culture, the actin filaments in cells were stained with green fluorescence (Alexa Fluor 488 Phalloidin) to show that the cells were able to attach, spread, and grow within the spaces between the capsules in the multiscale system. In addition, the nanoparticles (containing rhodamine B with red fluorescence) mainly stayed inside the capsules (Figure 2b). Some red fluorescence of rhodamine B could be seen in the ADSCs, indicating rhodamine B and possibly EGF were released from the nano-in-micro capsules.

To understand the effect of the composite hydrogel of EGF (E)-laden nano-in-micro capsules and ADSCs (A) in CH (NP-E@BM&A@CH) on cell proliferation, it was compared with ADSCs in CH (A@CH), EGF-laden nanoparticles and ADSCs

DOI: 10.1021/acscentsci.7b00213
ACS Cent. Sci. 2017, 3, 875–885

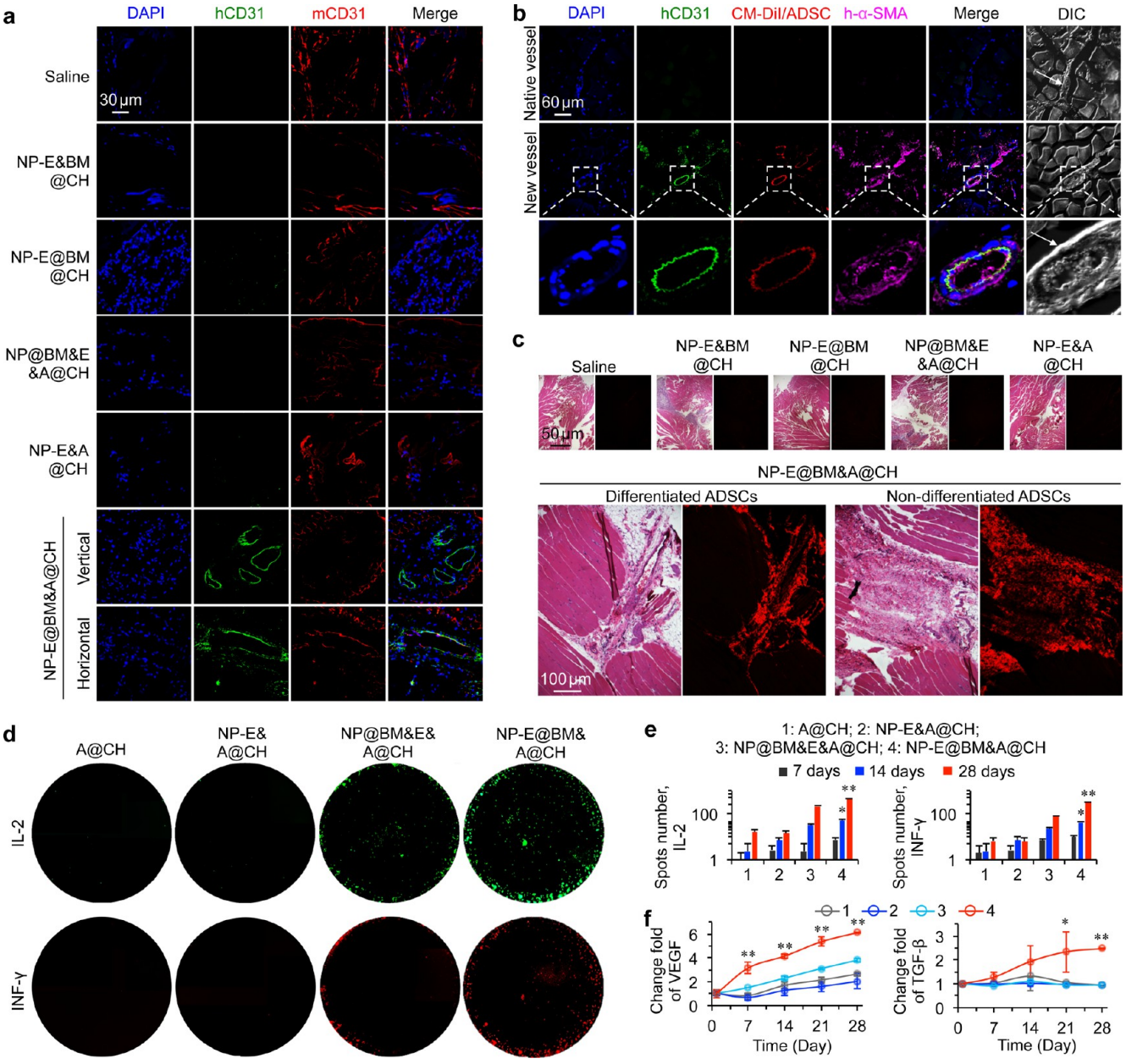

Figure 4. Mechanism of the multiscale composite system for augmented regeneration of ischemic limb. (a) The staining of human CD31 (hCD31) and mouse CD31 (mCD31) shows that some of the blood vessels in the NP-E@BM&A@CH treated mice are of human origin, which should be differentiated from the implanted human ADSCs. This is not observed in the five control groups. (b) Further confirmation of new blood vessels originated from implanted human ADSCs in the NP-E@BM&A@CH treated mice by using CellTracker CM-DiI dye labeled human ADSCs and staining with hCD31 and human α-SMA (h-α-SMA). (c) H&E staining and fluorescence images of tissue sections showing only the NP-E@BM&A@CH treatment effectively retained the ADSCs at the injection sites at 4 weeks after implantation. Both differentiated and nondifferentiated ADSCs were observable in the images. (d–e) Images (d) and quantitative data (e) from fluoroSpot studies of IL-2 and INF-γ secretion by ADSCs in collagen hydrogel (CH) (A@CH), EGF-laden nanoparticles and ADSCs in CH (NP-E&A@CH), empty nano-in-micro capsules mixed with free EGF and ADSCs in CH (NP@BM&E&A@CH), and EGF-laden nano-in-micro capsules and ADSCs in CH (NP-E@BM&A@CH), showing cells in the NP-E@BM&A@CH group exhibit significantly higher production of the IL-2 and INF-γ than cells in all the other control groups after day 14. (f) ELISA data of both vascular endothelial growth factor (VEGF) and transforming growth factor-beta (TGF-β) showing significantly higher levels of the two growth factors produced by cells in NP-E@BM&A@CH than all the other groups. Error bars represent s.d. ($n = 3$). $^{**}p < 0.01$ and $^{*}p < 0.05$ (Kruskal–Wallis H-test).

in CH (NP-E&A@CH), empty nano-in-micro capsules mixed with free EGF and ADSCs in CH (NP@BM&E&A@CH). As shown in Figure 2c, phalloidin (green) stained ADSCs in A@CH and NP-E&A@CH groups were mainly located on the surface of the scaffolds after one-day culture. Moreover, the CH shrank more than 8 times after a one-day culture (Figure S11), which might limit the diffusion of nutrients into the interior of the CH. In stark contrast, the composite hydrogel with nano-in-micro capsules did not shrink much at all, and the cells were observed to distribute homogeneously throughout the system (Figure 2c and Figure S11). The live and dead stains showed that many ADSCs in A@CH and NP-E&A@CH were dead (Figure S12), which could be due to the shrinkage of CH.[46] Overall, significantly more cells were observed inside the NP-E@BM&A@CH than all

DOI: 10.1021/acscentsci.7b00213
ACS Cent. Sci. 2017, 3, 875–885

the other three conditions on days 6 and 9 (Figure 2d). Considering that the cells might experience hypoxia after *in vivo* implantation, we further checked the cell proliferation in a hypoxic environment (5% O_2). Similarly, proliferation of ADSCs was significantly enhanced in the NP-E@BM&A@CH group on days 6 and 9 compared with all the three control groups (Figure S13). Figure 2e shows the sustained release of EGF from NP-E@BM into medium over a period of more than 300 h, while free EGF could be degraded quickly (in ~60 h) in medium at 37 °C. Although a sustained release of EGF could be achieved by encapsulating it in the nanoparticles alone, the ADSCs could readily take up the nanoparticles to minimize the binding of EGF to the EGFR on the cell surface. Indeed, when the ADSCs were cultured with NP-RC and NP-RC@BM, the fluorescence of curcumin (green) and rhodamine B (red) in NP-RC colocated with the fluorescence (blue) of lysoTracker that stained lysosomes/endosomes (Figure 2f). This indicated that the cells could take up the nanoparticles via endocytosis. In contrast, the distribution of fluorescence in cells treated with NP-RC@BM was similar to that of free Rho B & Cur (Figure 2f), indicating rhodamine B and curcumin were released from the nano-in-micro capsules before their interactions with cells. These data indicate that both maintaining the initial porosity of the CH by the nano-in-micro capsules and the sustained release of growth factor (EGF) from the capsules promote cell adhesion, survival, and proliferation inside the multiscale delivery system.

Therapy of Ischemic Limb with the Multiscale System *in Vivo*. The murine hind-limb ischemia model was used to evaluate the capability of the multiscale system for therapy of ischemic diseases. The ischemia was induced by unilateral femoral artery ligation as shown in Figure 3a. A laser Doppler perfusion imaging (LDPI) system was used to noninvasively quantify blood perfusion in the ischemic limbs. The blood perfusion in both limbs was normal before surgery, and it was reduced dramatically in the right limb immediately after the induction of ischemia on day 0 (Figure 3b). After confirmation of successful surgery, a total of 100 μL of saline, simple mixture of EGF-laden nanoparticles (NP-E) and bead microcapsules (BM) in CH (NP-E&BM@CH), NP-E@BM in CH (NP-E@BM@CH), NP@BM with free EGF and ADSCs in CH (NP@BM&E&A@CH), NP-E with ADSCs in CH (NP-E&A@CH), and NP-E@BM with ADSCs in CH (NP-E@BM&A@CH), were evenly injected into the ischemic area at five different locations immediately. The LDPI images were taken at different days for all the groups, which shows that the restoration of blood perfusion in the hind limb was faster in mice with the NP-E@BM&A@CH (i.e., the multiscale system) treatment than all the other treatments (Figure 3b). This difference was statistically significant after day 7 (Figure 3c). It is worth noting that the materials, EGF, and/or ADSCs all improved the blood perfusion compared with saline. More importantly, the multiscale system was the best for restoring the blood perfusion. However, with the surgical procedure performed in this study, no limb ischemia-associated complication including digital necrosis and unhealing ulcer[47−49] was observed in the wild-type mice even with saline treatment. This is probably because the wild-type mice have some inherent capacity of healing ischemic injury as shown by the blood perfusion data for the saline treatment (Figure 3b−c). This is not surprising because the recovery of vascular perfusion and function of the ischemic limbs in mouse models is largely determined by the surgical procedure and genetic backgrounds of mice.[50,51] In order to check if the multiscale system could prevent the complications of limb ischemia, the heterozygous *Akt1* knockout (KO) mice were treated in the same way as that shown in Figure 3a−b for saline and the three treatment groups with ADSCs. This is because Akt1 signaling plays a critical role in ischemia-induced angiogenesis and circulation recovery.[52] Indeed, as shown in Figure S14, digital necrosis and/or unhealing ulcer were observed at 4 weeks for one of the three *Akt1* KO mice treated with saline, NP-E&A@CH, or NP@BM&E&A@CH, while no such complications were seen for the three *Akt1* KO mice treated with NP-E@BM&A@CH (i.e., the multiscale system).

Since the induction of ischemia in the hind limb could lead to remarkable muscle degeneration,[53] we next examined the hematoxylin and eosin (H&E) staining of the limb muscle. The results show that the muscle fibers became largely disconnected in all the groups except the NP-E@BM&A@CH group (Figure 3d). The mean muscle fiber area determined from the H&E images (Figure 3e) and the staining of actin and fibronectin (Figure 3f) also show that the NP-E@BM&A@CH treatment resulted in the longest and largest muscle fibers. Furthermore, the NP-E@BM&A@CH treatment significantly reduced fibrosis (Figure S15) compared with all other treatments at 28 days after injection. Interestingly, we also noticed newly formed blood vessels at the injection area (encircled by the dashed line) for the NP-E@BM&A@CH treated group while the injection area is largely empty for all the other treatments (Figure 3g). More importantly, red blood cells could be seen in the new vessels (Figure 3g), indicating blood perfusion in the vessels. Equally important, we did not notice any evident side effect of the NP-E@BM&A@CH treatment. No mice died during all the experiments. Major organs from mice in the NP-E@BM&A@CH group were collected on day 28 for histology analysis. No obvious damage to the critical organs was observable in the H&E stained tissue slices (Figure S16). These results suggest excellent safety of the NP-E@BM&A@CH treatment *in vivo*.

Mechanisms of Enhancing Ischemic Limb Therapy with the Multiscale System. Since newly formed blood vessels were observed in the H&E stained tissue, we next sought to investigate the origin of the new vessels in the ischemic limb. As the ADSCs used in this study were from normal (nondiabetic) human adult lipoaspirates collected during elective surgical liposuction procedures, we used both human CD31 (hCD31) and mouse CD31 (mCD31) antibodies to determine if the newly formed blood vessels were formed due to differentiation of the implanted human ADSCs.[54,55] The fluorescence images show that the NP-E@BM&A@CH treated mice indeed had blood vessels that were positive for hCD31, which was not observed in all the other groups (Figure 4a). To further confirm this, we used the CellTracker CM-DiI (red fluorescent dye) labeled ADSCs for implantation. In saline, BM&NP@CH, NP-E@BM@CH, NP@BM&E&A@CH, and NP-E&A@CH treated groups, we did not observe any red fluorescence of the DiI dye at 28 days after implantation (Figure S17). In contrast, we observed some DiI-labeled cells in the blood vessels in the ischemic region of NP-E@BM&A@CH treated mice (Figure 4b). Furthermore, these blood vessels could be labeled with hCD31 and human α-SMA (h-α-SMA), indicating that the blood vessels were newly formed and matured from the implanted ADSCs (Figure 4b).[56] As a control, we also observed blood vessels in NP-E@BM&A@CH treated mice that were not stained with hCD31 or h-α-SMA, suggesting that these were the native blood vessels in the mouse (Figure 4b).

The H&E staining of the limb tissue injected with DiI-labeled ADSCs also show that only NP-E@BM&A@CH treated group

DOI: 10.1021/acscentsci.7b00213
ACS Cent. Sci. 2017, 3, 875−885

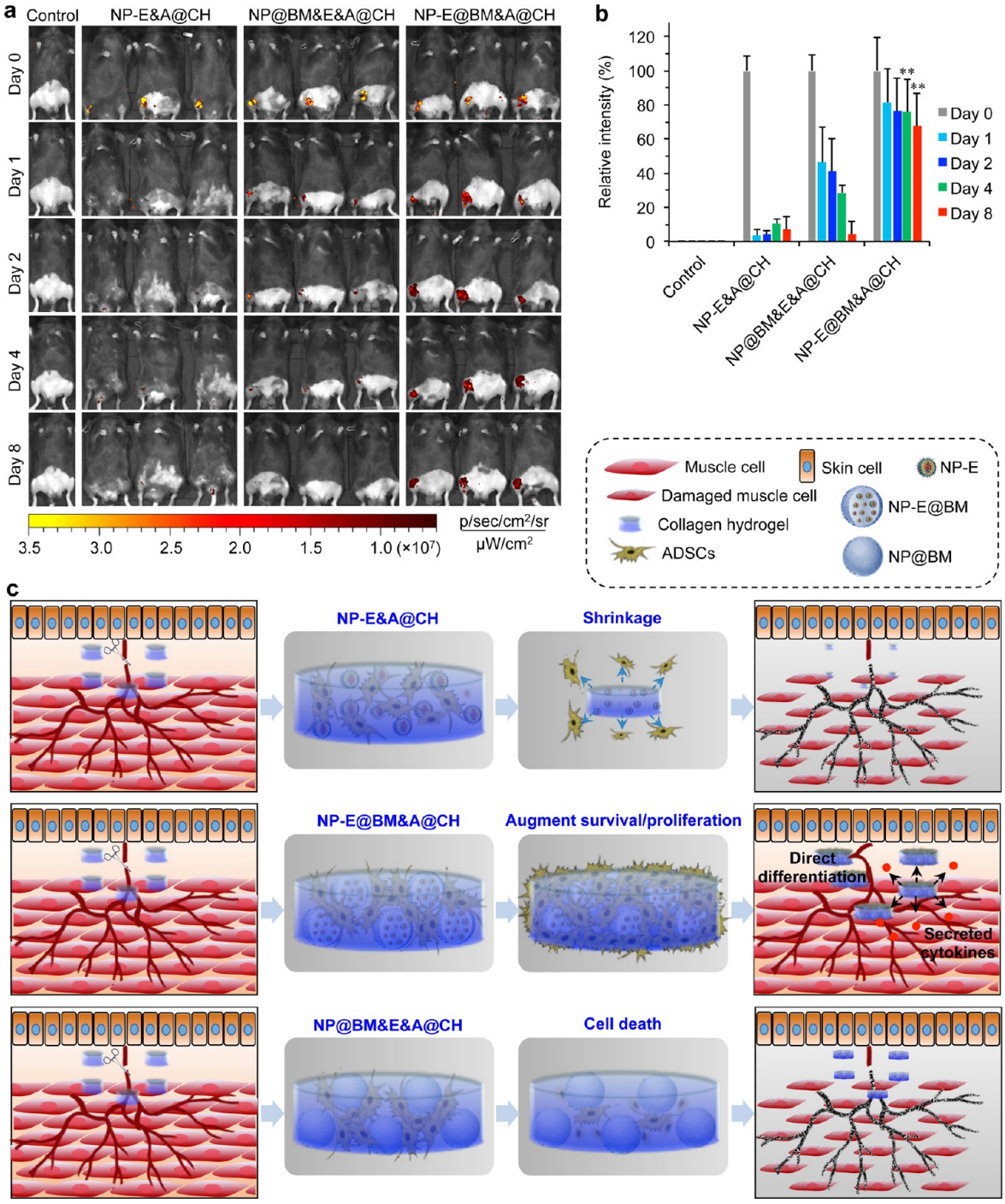

Figure 5. Significantly enhanced *in vivo* survival of ADSCs implanted with the multiscale system. The ADSCs were stained with CellTracker CM-DiI dye before injecting into the right legs (with surgery) of mice. (a) IVIS whole animal images. (b) Quantitative data. NP-E&A@CH: EGF (E) encapsulated nanoparticles (NP-E) and ADSCs (A) in collagen hydrogel (CH), NP@BM&E&A@CH: empty nano-in-micro capsules mixed with free EGF and ADSCs in CH, and the multiscale system NP-E@BM&A@CH: EGF encapsulated nano-in-micro capsules and ADSCs in CH. Error bars represent s.d. (n = 3). **p < 0.01 (Kruskal–Wallis H-test), for comparisons between the multiscale system and the two conventional systems with EGF-laden nanoparticles and hydrogel. On day 8 after implantation, the multiscale system improves the stem cell survival to ~70% from ~4–7% for the two conventional systems. (c) A schematic illustration of the enhanced survival of ADSCs in EGF-laden nano-in-micro system (NP-E@BM&A@CH) compared with EGF-laden nanoparticle system (NP-E&A@CH) and EGF-laden collagen hydrogel system with empty nano-in-micro capsules (NP@BM&E&A@CH). Ultimately, the multiscale composite system leads to significantly higher stem cell survival, better restoration of blood perfusion, and denser muscle structure.

exhibited strong fluorescence of DiI (Figure 4c). Interestingly, we could see that the cells with fluorescence were in two different stages. First, the cells were present in the newly formed blood vessels as aforementioned, suggesting that some of the implanted ADSCs differentiated into endothelial cells and contributed to the new blood vessel formation. This confirms the observation at the injection area of the NP-E@BM&A@CH treatment shown in Figure 3g. Second, the cells were observed in the hydrogel-

DOI: 10.1021/acscentsci.7b00213
ACS Cent. Sci. 2017, 3, 875–885

liked area in muscles, suggesting that some of the implanted ADSCs stayed within the hydrogel after implantation (Figure 4c). As stem cells could repair or regenerate damaged tissues/organs by either direct differentiation or indirectly via producing regenerative molecules such as growth factors and cytokines,[57,58] we further checked the secretion of these bioactive molecules from the ADSCs. Dual cytokine fluorospot analysis of human IL-2 and INF-γ was used to determine the effect of nano-in-micro capsules on the production of cytokines in ADSCs. As shown in Figures 4d–e and S18, stem cells in the NP-E@BM&A@CH had significantly higher production of IL-2 and INF-γ than the cells in all other groups starting from day 14. These cytokines were reported to be involved in tissue regeneration.[59,60] Stem cells could also secrete growth factors to facilitate the repair of injured tissue.[57,61] Indeed, ELISA analyses show that the production of both VEGF and TGF-β by the cells in the NP-E@BM&A@CH group was significantly elevated compared with all the other control groups (Figure 4f). VEGF and TGF-β are known to be important for blood vessel formation, and cell growth, proliferation, and differentiation. It is worth noting that although the multiscale system is expected to stay at the injection area, the cytokines and growth factors produced by ADSCs could be released from the system and carried away by body fluid including circulating blood to exert their systematic effect. On the basis of these results, we could conclude that the implanted ADSCs in the multiscale system (i.e., NP-E@BM&A@CH) could participate in the formation of new blood vessels via both direct endothelial differentiation and modulation of the microenvironment in the ischemic tissue by secreting cytokines and growth factors to promote blood vessel formation. However, it is unclear which one of the two mechanisms plays a dominant role in the process of angiogenesis and restoration of circulation in limb ischemia. Future studies are needed to further define the role of the two mechanisms.

Lastly, we labeled the ADSCs with CellTracker CM-DiI for implantation to check their survival *in vivo* in the ischemic limbs of mice. As shown in Figure 5a, fluorescence at the injection sites was evident in mice treated with NP-E@BM&A@CH even after 8 days of implantation, while it rapidly decreased in 1–4 days and was barely detectable on day 8 post implantation for the two control treatments with ADSCs (i.e., NP-E&A@CH and NP@BM&E&A@CH). Quantitative analyses of the fluorescence intensity showed that ~70% of the ADSCs implanted with the multiscale system survived after 8 days, compared to ~4–7% for the NP-E&A@CH (EGF encapsulated in nanoparticles for delivery) and NP@BM&E&A@CH (free EGF in collagen hydrogel for delivery) treatments (Figure 5b). The latter is similar to that reported in the literature for stem cell injection into ischemic limb.[17,18] This survival data may explain why the injection area is largely empty for all the treatments except the NP-E@BM&A@CH, as shown in Figure 3g. It is worth noting that although ADSCs may secret EGF,[62] the amount of the self-secreted EGF may not be enough to promote their survival and proliferation at the early stage after injection *in vivo* (Figure 5). Consistent with the literature,[63] the sustained release of EGF from the nano-in-micro system could augment the survival and proliferation of ADCSs both *in vivo* and *in vitro* (Figures 2d and 5). Moreover, the existence of exogenous EGF could enhance the secretion of angiogenic factors by ADSCs.[64] Therefore, the sustained release of extracellular EGF around ADSCs is important for the therapy of ischemic diseases. The main challenge of using stem cells is to keep them alive and functional in the target region after implantation. Our multiscale composite system may provide a unique solution to this grand challenge.

CONCLUSIONS

In summary, we have developed a novel multiscale composite system consisting of ADSCs, EGF-laden nano-in-micro capsules, and collagen hydrogel. This system can be used to achieve a sustained and localized release of EGF in the extracellular space, which enables its enhanced interactions with stem cells. In contrast, the nanoparticle-encapsulated EGF could be easily taken up by cells, while free EGF in collagen hydrogel or EGF encapsulated in alginate hydrogel microcapsules could be quickly degraded, which compromises its function of interacting with the EGFR on the cell surface. Moreover, unlike nanoparticles, the nano-in-micro capsules can minimize the shrinkage of the collagen hydrogel, allowing for homogeneous growth of stem cells in the multiscale system. As a result, the stem cell survival after implantation can be greatly enhanced compared to the conventional nanoparticle and hydrogel systems. As illustrated in Figure 5c, the ADSCs delivered in the multiscale composite system contribute to the formation of new blood vessels *in vivo* with direct differentiation into endothelial cells. Furthermore, the ADSCs can secrete cytokines and growth factors that promote regeneration and healing in the ischemic hind limb. Ultimately, the multiscale composite system leads to effective restoration of ~100% blood perfusion in 4 weeks and preservation of muscle in the ischemic limb. Collectively, the present work provides a new strategy of stem cell delivery with great potential for treating ischemic diseases.

ASSOCIATED CONTENT

Supporting Information

The Supporting Information is available free of charge on the ACS Publications website at DOI: 10.1021/acscentsci.7b00213.

Experimental details on preparation of nanoparticles and nano-in-micro capsules, drug encapsulation and release, *in vitro* cell imaging and cell viability, *in vivo* animal study, Masson's trichrome and immunohistochemical staining, detection of cytokines and growth factors. Supporting Figures S1–S18 (PDF)

AUTHOR INFORMATION

Corresponding Authors

*(X.H.) E-mail: he.429@osu.edu.

*(Z.L.) E-mail: zhenguo.liu@osumc.edu.

ORCID

Xiaoming He: 0000-0003-0125-6086

Author Contributions

◆H.W., P.A., and Y.X. contributed equally to this work.

Funding

This work was partially supported by NIH (R01EB023632, R01AI123661, R01HL094650, R01ES026200, and R01HL124122), NSF (CBET-1605425), and a James Hay and Ruth Jansson Wilson Professorship to Z.L.

Notes

The authors declare no competing financial interest.

REFERENCES

(1) Luttun, A.; Tjwa, M.; Moons, L.; Wu, Y.; Angelillo-Scherrer, A.; Liao, F.; Nagy, J. A.; Hooper, A.; Priller, J.; De Klerck, B. Revascularization of Ischemic Tissues by Plgf Treatment, and Inhibition

DOI: 10.1021/acscentsci.7b00213
ACS Cent. Sci. 2017, 3, 875–885

of Tumor Angiogenesis, Arthritis and Atherosclerosis by Anti-Flt1. *Nat. Med.* **2002**, *8*, 831−840.
(2) Carmeliet, P. Angiogenesis in Health and Disease. *Nat. Med.* **2003**, *9*, 653−660.
(3) Zhao, S.; Xu, Z.; Wang, H.; Reese, B. F.; Gushchina, L.; Jiang, M.; Agarwal, P.; Xu, J.; Zhang, M.; Shen, R.; Liu, Z.; Weisleder, N.; He, X. Bioengineering of Injectable Encapsulated Aggregates of Pluripotent Stem Cells for Therapy of Myocardial Infarction. *Nat. Commun.* **2016**, *7*, 13306.
(4) Murohara, T.; Asahara, T.; Silver, M.; Bauters, C.; Masuda, H.; Kalka, C.; Kearney, M.; Chen, D.; Symes, J.; Fishman, M.; Huang, P. L.; Isner, J. M. Nitric Oxide Synthase Modulates Angiogenesis in Response to Tissue Ischemia. *J. Clin. Invest.* **1998**, *101*, 2567−2578.
(5) Semenza, G. L. Hypoxia-Inducible Factors in Physiology and Medicine. *Cell* **2012**, *148*, 399−408.
(6) Menon, B. K.; Campbell, B. C.; Levi, C.; Goyal, M. Role of Imaging in Current Acute Ischemic Stroke Workflow for Endovascular Therapy. *Stroke* **2015**, *46*, 1453−1461.
(7) Robinton, D. A.; Daley, G. Q. The Promise of Induced Pluripotent Stem Cells in Research and Therapy. *Nature* **2012**, *481*, 295−305.
(8) Bianco, P.; Cao, X.; Frenette, P. S.; Mao, J. J.; Robey, P. G.; Simmons, P. J.; Wang, C.-Y. The Meaning, the Sense and the Significance: Translating the Science of Mesenchymal Stem Cells into Medicine. *Nat. Med.* **2013**, *19*, 35−42.
(9) Tang, J.; Shen, D.; Caranasos, T. G.; Wang, Z.; Vandergriff, A. C.; Allen, T. A.; Hensley, M. T.; Dinh, P. U.; Cores, J.; Li, T. S.; Zhang, J.; Kan, Q.; Cheng, K. Therapeutic Microparticles Functionalized with Biomimetic Cardiac Stem Cell Membranes and Secretome. *Nat. Commun.* **2017**, *8*, 13724.
(10) Mizuno, H.; Tobita, M.; Uysal, A. C. Concise Review: Adipose-Derived Stem Cells as a Novel Tool for Future Regenerative Medicine. *Stem Cells* **2012**, *30*, 804−810.
(11) Krawiec, J. T.; Vorp, D. A. Adult Stem Cell-Based Tissue Engineered Blood Vessels: A Review. *Biomaterials* **2012**, *33*, 3388−3400.
(12) Lee, S.; Choi, E.; Cha, M.-J.; Hwang, K.-C. Cell Adhesion and Long-Term Survival of Transplanted Mesenchymal Stem Cells: A Prerequisite for Cell Therapy. *Oxid. Med. Cell. Longevity* **2015**, *2015*, 632902.
(13) Li, X.; Tamama, K.; Xie, X.; Guan, J. Improving Cell Engraftment in Cardiac Stem Cell Therapy. *Stem Cells Int.* **2016**, *2016*, 7168797.
(14) Arno, A.; Smith, A. H.; Blit, P. H.; Shehab, M. A.; Gauglitz, G. G.; Jeschke, M. G. Stem Cell Therapy: A New Treatment for Burns? *Pharmaceuticals* **2011**, *4*, 1355−1380.
(15) Ishii, T. Fetal Stem Cell Transplantation: Past, Present, and Future. *World J. Stem Cell.* **2014**, *6*, 404−420.
(16) Speidel, A. T.; Stuckey, D. J.; Chow, L. W.; Jackson, L. H.; Noseda, M.; Abreu Paiva, M.; Schneider, M. D.; Stevens, M. M. Multimodal Hydrogel-Based Platform to Deliver and Monitor Cardiac Progenitor/Stem Cell Engraftment. *ACS Cent. Sci.* **2017**, *3*, 338−348.
(17) Beegle, J. R.; Magner, N. L.; Kalomoiris, S.; Harding, A.; Zhou, P.; Nacey, C.; White, J. L.; Pepper, K.; Gruenloh, W.; Annett, G.; Nolta, J. A.; Fierro, F. A. Preclinical Evaluation of Mesenchymal Stem Cells Overexpressing Vegf to Treat Critical Limb Ischemia. *Mol. Ther.–Methods Clin. Dev.* **2016**, *3*, 16053.
(18) van der Bogt, K. E.; Hellingman, A. A.; Lijkwan, M. A.; Bos, E. J.; de Vries, M. R.; van Rappard, J. R.; Fischbein, M. P.; Quax, P. H.; Robbins, R. C.; Hamming, J. F.; Wu, J. C. Molecular Imaging of Bone Marrow Mononuclear Cell Survival and Homing in Murine Peripheral Artery Disease. *JACC Cardiovasc. Imaging* **2012**, *5*, 46−55.
(19) Benoit, E.; O'Donnell, T. F.; Iafrati, M. D.; Asher, E.; Bandyk, D. F.; Hallett, J. W.; Lumsden, A. B.; Pearl, G. J.; Roddy, S. P.; Vijayaraghavan, K.; Patel, A. N. The Role of Amputation as an Outcome Measure in Cellular Therapy for Critical Limb Ischemia: Implications for Clinical Trial Design. *J. Transl. Med.* **2011**, *9*, 165.
(20) Mamidi, M. K.; Pal, R.; Dey, S.; Bin Abdullah, B. J. J.; Zakaria, Z.; Rao, M. S.; Das, A. K. Cell Therapy in Critical Limb Ischemia: Current Developments and Future Progress. *Cytotherapy* **2012**, *14*, 902−916.
(21) Aranguren, X. L.; Verfaillie, C. M.; Luttun, A. Emerging Hurdles in Stem Cell Therapy for Peripheral Vascular Disease. *J. Mol. Med.* **2009**, *87*, 3−16.
(22) Ouma, G. O.; Zafrir, B.; Mohler, E. R.; Flugelman, M. Y. Therapeutic Angiogenesis in Critical Limb Ischemia. *Angiology* **2013**, *64*, 466−480.
(23) Discher, D. E.; Mooney, D. J.; Zandstra, P. W. Growth Factors, Matrices, and Forces Combine and Control Stem Cells. *Science* **2009**, *324*, 1673−1677.
(24) Chen, G.; Gulbranson, D. R.; Yu, P.; Hou, Z.; Thomson, J. A. Thermal Stability of Fibroblast Growth Factor Protein Is a Determinant Factor in Regulating Self-Renewal, Differentiation, and Reprogramming in Human Pluripotent Stem Cells. *Stem Cells* **2012**, *30*, 623−630.
(25) Farokhzad, O. C.; Langer, R. Impact of Nanotechnology on Drug Delivery. *ACS Nano* **2009**, *3*, 16−20.
(26) Panyam, J.; Labhasetwar, V. Biodegradable Nanoparticles for Drug and Gene Delivery to Cells and Tissue. *Adv. Drug Delivery Rev.* **2003**, *55*, 329−347.
(27) Bai, T.; Liu, F.; Zou, F.; Zhao, G.; Jiang, Y.; Liu, L.; Shi, J.; Hao, D.; Zhang, Q.; Zheng, T.; Zhang, Y.; Liu, M.; Li, S.; Qi, L.; Liu, J. Y. Epidermal Growth Factor Induces Proliferation of Hair Follicle-Derived Mesenchymal Stem Cells through Epidermal Growth Factor Receptor-Mediated Activation of Erk and Akt Signaling Pathways Associated with Upregulation of Cyclin D1 and Downregulation of P16. *Stem Cells Dev.* **2017**, *26*, 113−122.
(28) Zhang, X.; Wang, Y.; Gao, Y.; Liu, X.; Bai, T.; Li, M.; Li, L.; Chi, G.; Xu, H.; Liu, F.; Liu, J. Y.; Li, Y. Maintenance of High Proliferation and Multipotent Potential of Human Hair Follicle-Derived Mesenchymal Stem Cells by Growth Factors. *Int. J. Mol. Med.* **2013**, *31*, 913−921.
(29) Wang, H.; Agarwal, P.; Zhao, S.; Xu, R. X.; Yu, J.; Lu, X.; He, X. Hyaluronic Acid-Decorated Dual Responsive Nanoparticles of Pluronic F127, Plga, and Chitosan for Targeted Co-Delivery of Doxorubicin and Irinotecan to Eliminate Cancer Stem-Like Cells. *Biomaterials* **2015**, *72*, 74−89.
(30) Wang, H.; Agarwal, P.; Zhao, S.; Yu, J.; Lu, X.; He, X. A near-Infrared Laser-Activated "Nanobomb" for Breaking the Barriers to Microrna Delivery. *Adv. Mater.* **2016**, *28*, 347−355.
(31) Wang, H.; Zhao, S.; Agarwal, P.; Dumbleton, J.; Yu, J.; Lu, X.; He, X. Multi-Layered Polymeric Nanoparticles for Ph-Responsive and Sequenced Release of Theranostic Agents. *Chem. Commun.* **2015**, *51*, 7733−7736.
(32) Agarwal, P.; Zhao, S.; Bielecki, P.; Rao, W.; Choi, J. K.; Zhao, Y.; Yu, J.; Zhang, W.; He, X. One-Step Microfluidic Generation of Pre-Hatching Embryo-Like Core−Shell Microcapsules for Miniaturized 3d Culture of Pluripotent Stem Cells. *Lab Chip* **2013**, *13*, 4525−4533.
(33) Hoffman, A. S. Hydrogels for Biomedical Applications. *Ann. N. Y. Acad. Sci.* **2001**, *944*, 62−73.
(34) Alsberg, E.; Anderson, K. W.; Albeiruti, A.; Rowley, J. A.; Mooney, D. J. Engineering Growing Tissues. *Proc. Natl. Acad. Sci. U. S. A.* **2002**, *99*, 12025−12030.
(35) Zhao, S.; Zhang, L.; Han, J.; Chu, J.; Wang, H.; Chen, X.; Wang, Y.; Tun, N.; Lu, L.; Bai, X. F.; Yearsley, M.; Devine, S.; He, X.; Yu, J. Conformal Nanoencapsulation of Allogeneic T Cells Mitigates Graft-Versus-Host Disease and Retains Graft-Versus-Leukemia Activity. *ACS Nano* **2016**, *10*, 6189−6200.
(36) Lee, K. Y.; Mooney, D. J. Hydrogels for Tissue Engineering. *Chem. Rev.* **2001**, *101*, 1869−1879.
(37) Augst, A. D.; Kong, H. J.; Mooney, D. J. Alginate Hydrogels as Biomaterials. *Macromol. Biosci.* **2006**, *6*, 623−633.
(38) Huang, H.; He, X. Fluid Displacement During Droplet Formation at Microfluidic Flow-Focusing Junction. *Lab Chip* **2015**, *15*, 4197−4205.
(39) Hoffman, A. S. Hydrogels for Biomedical Applications. *Adv. Drug Delivery Rev.* **2012**, *64*, 18−23.
(40) Gombotz, W. R.; Wee, S. F. Protein Release from Alginate Matrices. *Adv. Drug Delivery Rev.* **2012**, *64*, 194−205.
(41) Li, Y.-P.; Pei, Y.-Y.; Zhang, X.-Y.; Gu, Z.-H.; Zhou, Z.-H.; Yuan, W.-F.; Zhou, J.-J.; Zhu, J.-H.; Gao, X.-J. Pegylated Plga Nanoparticles as

DOI: 10.1021/acscentsci.7b00213
ACS Cent. Sci. 2017, 3, 875−885

Protein Carriers: Synthesis, Preparation and Biodistribution in Rats. *J. Controlled Release* **2001**, *71*, 203−211.
(42) Alonso-Sande, M.; des Rieux, A.; Fievez, V.; Sarmento, B.; Delgado, A.; Evora, C.; Remuñán-López, C.; Préat, V. r.; Alonso, M. J. Development of Plga-Mannosamine Nanoparticles as Oral Protein Carriers. *Biomacromolecules* **2013**, *14*, 4046−4052.
(43) Pakulska, M. M.; Donaghue, I. E.; Obermeyer, J. M.; Tuladhar, A.; McLaughlin, C. K.; Shendruk, T. N.; Shoichet, M. S. Encapsulation-Free Controlled Release: Electrostatic Adsorption Eliminates the Need for Protein Encapsulation in Plga Nanoparticles. *Sci. Adv.* **2016**, *2*, e1600519.
(44) Narhi, L. O.; Arakawa, T.; Mcginley, M. D.; Rohde, M. F.; Westcott, K. R. Circular Dichroism of Reduced and Oxidized Recombinant Human Epidermal Growth Factor. *Int. J. Pept. Protein Res.* **1992**, *39*, 182−187.
(45) Prestrelski, S.; Arakawa, T.; Wu, C.; O'Neal, K.; Westcott, K.; Narhi, L. Solution Structure and Dynamics of Epidermal Growth Factor and Transforming Growth Factor Alpha. *J. Biol. Chem.* **1992**, *267*, 319−322.
(46) Choi, J. S.; Harley, B. A. Marrow-Inspired Matrix Cues Rapidly Affect Early Fate Decisions of Hematopoietic Stem and Progenitor Cells. *Sci. Adv.* **2017**, *3*, e1600455.
(47) Kidoya, H.; Naito, H.; Takakura, N. Apelin Induces Enlarged and Nonleaky Blood Vessels for Functional Recovery from Ischemia. *Blood* **2010**, *115*, 3166−3174.
(48) Lee, H. C.; An, S. G.; Lee, H. W.; Park, J.-S.; Cha, K. S.; Hong, T. J.; Park, J. H.; Lee, S. Y.; Kim, S.-P.; Kim, Y. D.; Chung, S. W.; Bae, Y. C.; Shin, Y. B.; Kim, J. I.; Jung, J. S. Safety and Effect of Adipose Tissue-Derived Stem Cell Implantation in Patients with Critical Limb Ischemia. *Circ. J.* **2012**, *76*, 1750−1760.
(49) Tateishi-Yuyama, E.; Matsubara, H.; Murohara, T.; Ikeda, U.; Shintani, S.; Masaki, H.; Amano, K.; Kishimoto, Y.; Yoshimoto, K.; Akashi, H.; et al. Therapeutic Angiogenesis for Patients with Limb Ischaemia by Autologous Transplantation of Bone-Marrow Cells: A Pilot Study and a Randomised Controlled Trial. *Lancet* **2002**, *360*, 427−435.
(50) Hellingman, A. A.; Bastiaansen, A. J.; de Vries, M. R.; Seghers, L.; Lijkwan, M. A.; Lowik, C. W.; Hamming, J. F.; Quax, P. H. Variations in Surgical Procedures for Hind Limb Ischaemia Mouse Models Result in Differences in Collateral Formation. *Eur. J. Vasc. Endovasc. Surg.* **2010**, *40*, 796−803.
(51) Shireman, P. K.; Quinones, M. P. Differential Necrosis Despite Similar Perfusion in Mouse Strains after Ischemia. *J. Surg. Res.* **2005**, *129*, 242−250.
(52) Ackah, E.; Yu, J.; Zoellner, S.; Iwakiri, Y.; Skurk, C.; Shibata, R.; Ouchi, N.; Easton, R. M.; Galasso, G.; Birnbaum, M. J.; Walsh, K.; Sessa, W. C. Akt1/Protein Kinase Balpha Is Critical for Ischemic and Vegf-Mediated Angiogenesis. *J. Clin. Invest.* **2005**, *115*, 2119−2127.
(53) Greco, S.; De Simone, M.; Colussi, C.; Zaccagnini, G.; Fasanaro, P.; Pescatori, M.; Cardani, R.; Perbellini, R.; Isaia, E.; Sale, P.; et al. Common Micro-Rna Signature in Skeletal Muscle Damage and Regeneration Induced by Duchenne Muscular Dystrophy and Acute Ischemia. *FASEB J.* **2009**, *23*, 3335−3346.
(54) Crosby, J. R.; Kaminski, W. E.; Schatteman, G.; Martin, P. J.; Raines, E. W.; Seifert, R. A.; Bowen-Pope, D. F. Endothelial Cells of Hematopoietic Origin Make a Significant Contribution to Adult Blood Vessel Formation. *Circ. Res.* **2000**, *87*, 728−730.
(55) DeLisser, H. M.; Newman, P. J.; Albelda, S. M. Molecular and Functional Aspects of Pecam-1/Cd31. *Immunol. Today* **1994**, *15*, 490−495.
(56) Bergers, G.; Song, S. The Role of Pericytes in Blood-Vessel Formation and Maintenance. *Neuro Oncol.* **2005**, *7*, 452−464.
(57) Kilroy, G. E.; Foster, S. J.; Wu, X.; Ruiz, J.; Sherwood, S.; Heifetz, A.; Ludlow, J. W.; Stricker, D. M.; Potiny, S.; Green, P.; et al. Cytokine Profile of Human Adipose-Derived Stem Cells: Expression of Angiogenic, Hematopoietic, and Pro-Inflammatory Factors. *J. Cell. Physiol.* **2007**, *212*, 702−709.
(58) Kim, W.-S.; Park, B.-S.; Sung, J.-H.; Yang, J.-M.; Park, S.-B.; Kwak, S.-J.; Park, J.-S. Wound Healing Effect of Adipose-Derived Stem Cells: A Critical Role of Secretory Factors on Human Dermal Fibroblasts. *J. Dermatol. Sci.* **2007**, *48*, 15−24.
(59) Liu, Y.; Wang, L.; Kikuiri, T.; Akiyama, K.; Chen, C.; Xu, X.; Yang, R.; Chen, W.; Wang, S.; Shi, S. M Mesenchymal stem cell-based tissue regeneration is governed by recipient T lymphocytes *via* IFN-γ and TNF-α. *Nat. Med.* **2011**, *17*, 1594−1601.
(60) Karin, M.; Clevers, H. Reparative Inflammation Takes Charge of Tissue Regeneration. *Nature* **2016**, *529*, 307−315.
(61) Daley, G. Q.; Scadden, D. T. Prospects for Stem Cell-Based Therapy. *Cell* **2008**, *132*, 544−548.
(62) Kalinina, N.; Kharlampieva, D.; Loguinova, M.; Butenko, I.; Pobeguts, O.; Efimenko, A.; Ageeva, L.; Sharonov, G.; Ischenko, D.; Alekseev, D.; et al. Characterization of Secretomes Provides Evidence for Adipose-Derived Mesenchymal Stromal Cells Subtypes. *Stem Cell Res. Ther.* **2015**, *6*, 221.
(63) Hamdan, S.; Pastar, I.; Drakulich, S.; Dikici, E.; Tomic-Canic, M.; Deo, S.; Daunert, S. Nanotechnology-Driven Therapeutic Interventions in Wound Healing: Potential Uses and Applications. *ACS Cent. Sci.* **2017**, *3*, 163−175.
(64) Li, Q.; Li, P.-H.; Hou, D.-J.; Zhang, A.-J.; Tao, C.-B.; Li, X.-Y.; Jin, P.-S. EGF enhances ADSCs secretion *via* ERK and JNK pathways. *Cell Biochem. Biophys.* **2014**, *69*, 189−196.

DOI: 10.1021/acscentsci.7b00213
ACS Cent. Sci. 2017, 3, 875−885